Vol 16 No 5, May 2007
1009-1963/2007/16(05)/1422-07

Chinese Physics

© 2007 Chin. Phys. Soc.
and IOP Publishing Ltd

Structural and electronic properties of Fe-doped $BaTiO_3$ and $SrTiO_3$*

Zhang Chao(张 超)†, Wang Chun-Lei(王春雷),
Li Ji-Chao(李吉超), and Yang Kun(杨 鲲)

School of Physics and Microelectronics, State Key Laboratory of Crystal Materials, Shandong University, Jinan 250100, *China*

(Received 19 July 2006; revised manuscript received 20 November 2006)

We have performed first principles calculations of Fe-doped $BaTiO_3$ and $SrTiO_3$. Dopant formation energy, structure distortion, band structure and density of states have been computed. The dopant formation energy is found to be 6.8 eV and 6.5 eV for Fe-doped $BaTiO_3$ and $SrTiO_3$ respectively. The distances between Fe impurity and its nearest O atoms and between Fe atom and Ba or Sr atoms are smaller than those of the corresponding undoped bulk systems. The Fe defect energy band is obtained, which mainly originates from Fe 3d electrons. The band gap is still an indirect one after Fe doping for both $BaTiO_3$ and $SrTiO_3$, but the gap changes from Γ–R point to Γ–X point.

Keywords: the first-principles, impurity, $BaTiO_3$, $SrTiO_3$
PACC: 7115M, 7155, 7115H

1. Introduction

Ferroelectric crystals, such as $SrTiO_3$, $BaTiO_3$, $KNbO_3$, etc., represent an important class of perovskite material with the interesting prospects of technological applications ranging from electronic ceramic to constituents in optical devices. Most of the chemical activities and physical properties of these materials can be enhanced through the introduction of extrinsic and intrinsic dopants, such as transition metal cations doping, excess oxygen and oxygen vacancies. Understanding the effect of dopant on the electronic structure would be a key step to the elucidation of these properties.[1−8] Therefore, the nature of defects in ABO_3 has been studied quite extensively both experimentally[1−5] and theoretically[9−12] in the last decades.

Strontium titanate ($SrTiO_3$) exhibits a mixed ionic–covalent chemical bonding, for the Sr–O bonds are quite ionic, while the Ti–O substructure is of partly covalent bond.[13] This nature of the chemical bonding leads to a unique structure, which makes it a model electronic material. Nevertheless, few theoretical calculations are devoted to a discussion on the properties of Fe-doped $SrTiO_3$.[9−11] From a tight-binding scheme together with the Green function method,[9] Selme *et al* deduced the shape of the optical transition spectra. The Fe acceptor level localized inside the $SrTiO_3$ band gap was found by Michel-Calendini and Muller using the $X\alpha$ cluster approach.[10] The recent calculations of Fe-doped $SrTiO_3$[11] have been performed using both periodic Hartree–Fock (HF) and density functional theory (DFT) based on the linear combination of atomic orbitals (LCAO) Gaussian basis sets. The results show the strong covalent bonding between unpaired electrons of the Fe impurity. Also it is found that four nearest O ions relax towards the impurity and the positions of Fe energy levels in a $SrTiO_3$ gap are very sensitive to the lattice relaxation.

Barium titanate ($BaTiO_3$) is another type of ABO_3 perovskite, which has not only large ferroelectric response, but also very large nonlinear optical and electro-optic coefficients, which is attractive to designing nonlinear optical devices. These properties can be dramatically enhanced when they are doped with transition metals.[3,14−16] Compared with $SrTiO_3$, the theoretical calculations on doping effect of $BaTiO_3$ are few. To our knowledge, there has been no theoretical study on Fe-doped cubic $BaTiO_3$ from first principles calculations.

The purpose of this paper is to throw some light

*Project supported by the National Basic Research Program of China (Grant No 2007CB607504) and the National Natural Science Foundation of China (Grant No 10474057).
†E-mail: zhangchao40@mail.sdu.edu.cn

on the influence of Fe impurity on the electronic and atomic structures in cubic phases of $BaTiO_3$ and $SrTiO_3$ perovskite from first principles calculations. The remainder of this paper is organized as follows. Section 2 contains the details of computational technique, including the theoretical methods and the supercell model. In Section 3, we present and discuss the computed dopant formation energy, lattice relaxation around impurity, and band gaps for both $BaTiO_3$ and $SrTiO_3$. Finally, a conclusion drawn from the present study is presented in Section 4.

2. Computational details

Our calculation is carried out using the ESPRESSO package,[17] which is based on the density functional theory using the plane-wave pseudopotential (PWP) formalism. The Local density approximation (LDA) with an ultra-soft pseudopotential is used. The Ceperley–Alder's exchange-correlation potential parametrized by the Perdew–Zunger scheme (CA–PZ)[18] is employed. Vanderbilt ultra-soft pseudopotentials[19] are adopted for each type of ion, in which the 5s, 5p and 6s electrons of Ba, the 4s, 4p and 5s electrons of Sr, the 3s, 3p, 3d and 4s electrons of Ti, the 2s and 2p electrons of O and the 3s, 3p, 3d, 4s and 4p electrons of Fe are all treated as valence states.

Firstly, we optimize the high-symmetric cubic (Pm3m) phases of $BaTiO_3$ and $SrTiO_3$ with $8 \times 8 \times 8$ Monkhorst–Pack[20] k-point mesh for the Brillouin zone integration. The cubic unit cell contains five atoms: one Ti atom at the cube centre, one Ba or Sr atom at the cube corner and three O atoms at the face centre. The computed lattice constants of $SrTiO_3$ in the LDA and general gradient approximation (GGA) are 3.85 Å and 3.93 Å, respectively, and are similar to the experimental value, 3.89 Å.[21] In the case of $BaTiO_3$, the theoretical lattice constant is 3.93 Å, which is only 1% smaller than the experimental one (4.00 Å),[21] whereas that in the GGA is 4.03 Å. So the difference between the lattice constants obtained using the LDA and GGA is slight. In the following calculations by ESPRESSO package, we use the computed lattice constants by LDA.[22,23]

Supercell model is adopted in our simulations,[11] with one Ti atom replaced by a Fe atom. Two kinds of supercells with sizes of 40-atom and 80-atom are used here, which represent 2.5% and 1.25% doping amount respectively. We extend the standard ABO_3-type primitive unit cell to the supercell with translation vectors obtained by a simple relation

$$A_j = \sum_{i=1}^{2} l_{ij} a_i, \tag{1}$$

where a_i is the translation vectors of the primitive cell. In our calculations, bulk Fe impurity structures are represented by supercells with the following extensions of the primitive unit cell vectors: $2 \times 2 \times 2$ and $2\sqrt{2} \times 2\sqrt{2} \times 2\sqrt{2}$, and the corresponding matrices are

$$A = \begin{pmatrix} 2 & 0 & 0 \\ 0 & 2 & 0 \\ 0 & 0 & 2 \end{pmatrix} \quad \text{and} \quad B = \begin{pmatrix} 2 & 2 & 0 \\ 2 & 0 & 2 \\ 0 & 2 & 2 \end{pmatrix}, \tag{2}$$

which result in the sc and fcc lattices respectively. For the first matrix, the constructed supercell consists of eight primitive perovskite unit cells and thus it contains $5 \times 8 = 40$ atoms. The supercell corresponding to matrix B contains 80 atoms. The distance between periodically repeated defects in the bulk is $2a_0$ for 40-atom supercell and $2\sqrt{2}a_0$ for 80-atom supercell, where a_0 is theoretical lattice constant. As the two kinds of supercells are highly symmetric, when we substitute Fe for any Ti atom in the supercell, we obtain the same value of E_f (defined below), 6.87 eV for a Fe-doped $BaTiO_3$ 40-atom system. This result shows that the impurity position has no influence on the results in our considered system.

Full relaxation with respect to the atomic positions is performed for doped systems with forces less than 1 mRyd/bohr. Before the geometry relaxation and property calculations, converging tests are carried out. And the plane-wave cutoff energy for the supercell is obtained to be 30 Ryd.

3. Results and discussion

3.1. Dopant formation energy

The dopant formation energy E_f of Fe impurity in the ABO_3 crystal is estimated using the following expression:[24]

$$E_f = E(ABO_3 + Fe) - E(ABO_3) + \mu_{Ti} - \mu_{Fe}, \tag{3}$$

where $E(ABO_3 + Fe)$ and $E(ABO_3)$ are energies of the doped and undoped crystal supercells, and μ_{Ti}

and μ_{Fe} are the chemical potentials per atom of Ti and Fe bulk crystal respectively. In other words, the dopant formation energy refers to the energy required to insert one Fe atom with a chemical potential μ_{Fe} into the supercell after removing one Ti atom from the same position. The chemical potentials are those of reference materials including titanium ($P6_3/mmc$) and iron ($Fm\bar{3}m$).

The dopant formation energies of $BaTiO_3$ and $SrTiO_3$ obtained from our calculations are listed in Table 1.

Table 1. The dopant formation energies of $BaTiO_3$ and $SrTiO_3$.

Supercell	40	80
k mesh	$4 \times 4 \times 4$	$3 \times 3 \times 3$
$E_f(BaTiO_3)$	6.87	6.82
$E_f(SrTiO_3)$	6.55	6.44

First we can see that the dopant formation energy weakly depends on the size of supercell. The larger supercell size corresponds to slightly lower formation energy for both $BaTiO_3$ and $SrTiO_3$. For $BaTiO_3$, the dopant formation energy varies from 6.87 to 6.82 eV when the supercell size increases from 40-atom to 80-atom, the difference is about 0.05 eV. This difference for Fe-doped $SrTiO_3$ system is 0.11 eV. Since in the case of doped system, the lower formation energy means that the system is more stable. Therefore the Fe doping amounts of 2.5% and 1.25% are nearly equally favourable from the viewpoint of formation energy. Another point can be seen from Table 1 is that the formation energies of Fe-doped $SrTiO_3$ are lower than those of $BaTiO_3$ for both 40-atom and 80-atom supercells, which indicates that the $SrTiO_3$ might be more easily doped with Fe than the $BaTiO_3$.

3.2. Lattice structure relaxation

The fully relaxed structure parameters of the doped systems are listed in Table 2 together with the parameters of the undoped bulk system for comparison. In Table 2 only the bond lengths near Fe atom are presented, the other lattice constants are the same as those of the undoped bulk system within the computation tolerance. Because of symmetry constraint, atoms behave identically in the x-, y- and z-directions. It can be clearly seen that the distances between Fe atom and its nearest O and between Fe atom and Ba or Sr atoms are smaller than those in the corresponding pure bulk materials. The six nearest O atoms shift towards the Fe atom about 0.04 Å in $BaTiO_3$ for the 40-atom supercell, and about 0.06 Å for the 80-atom supercell. However, the shift of Ba atoms towards Fe impurity is nearly the same (about 0.03 Å) for both the 40-atom and 80-atom supercells. This implies that the doped Fe atom has more influence on O atoms than on Ba atoms, since O atom is closer to Fe atom than to Ba atom. It is also interesting to notice from Table 2 that the change in distance around Fe atom in $SrTiO_3$ is nearly the same as that in Fe doped $BaTiO_3$.

Table 2. The change in distance around Fe atom in $SrTiO_3$ and in Fe doped $BaTiO_3$.

		$BaTiO_3$			$SrTiO_3$	
Ideal bulk	O–Ti	1.966		O–Ti	1.925	
	Ba–Ti	3.406		Sr–Ti	3.334	
40–atom	O–Fe	1.926	0.04 (1.0%)	O–Fe	1.883	0.04 (1.1%)
	Ba–Fe	3.378	0.03 (0.7%)	Sr–Fe	3.306	0.03 (0.7%)
80–atom	O–Fe	1.909	0.06 (1.4%)	O–Fe	1.871	0.05 (1.4%)
	Ba–Fe	3.373	0.03 (0.8%)	Sr–Fe	3.311	0.03 (0.6%)

The charge density maps for undoped and doped structures of $BaTiO_3$ and $SrTiO_3$ are shown in Fig.1 and Fig.2 respectively. Generally, the hybridization between O and B-site atoms (Ti or Fe) nearly has no change after being doped with Fe. From Fig.1 and Fig.2, we can see explicitly the Ti–O covalent bonding effect. On the other hand, the density maps drawn for (110) section (Fig.1(b) and Fig.2(b)) show no trace of the covalent bonding between the oxygen atom and Ba or Sr atom. The difference between the doped and the undoped charge density populations is marginal. The hybridization of Ti–O bond is slightly weakened, since the O shifts towards the Fe. The above discussion can be applied to both $BaTiO_3$ and $SrTiO_3$.

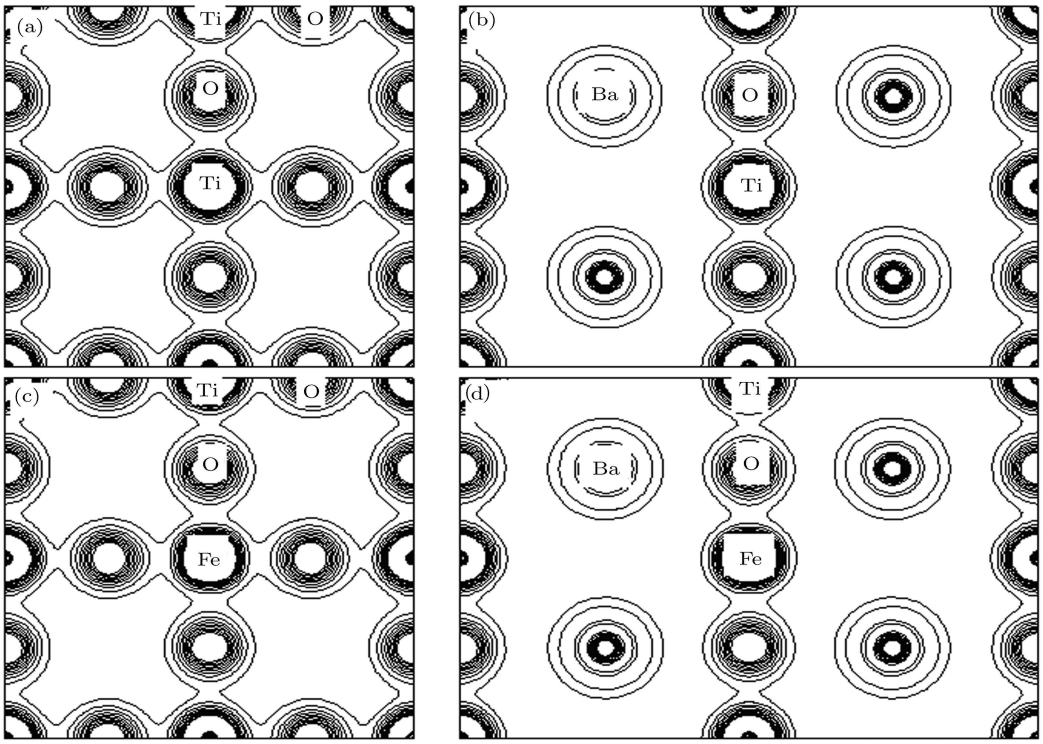


Fig.1. Charge density maps for undoped and Fe-doped $BaTiO_3$. The contour interval is 0.08 in atomic units. (a) the (001) section for undoped $BaTiO_3$, (b) the (110) section for undoped $BaTiO_3$, (c) the (001) section for doped $BaTiO_3$, (d) the (110) section for doped $BaTiO_3$.

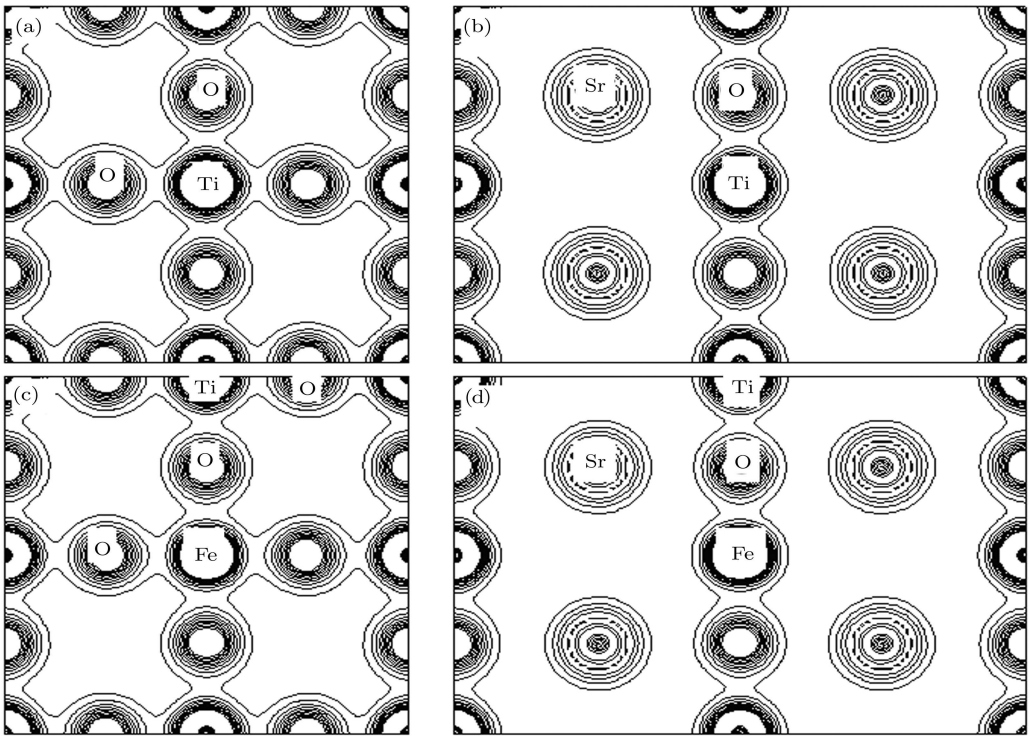


Fig.2. Charge density maps for undoped and Fe-doped $SrTiO_3$. The contour interval is 0.08 in atomic units. (a) the (001) section for undoped $SrTiO_3$, (b) the (110) section for undoped $SrTiO_3$, (c) the (001) section for doped $SrTiO_3$, (d) the (110) section for doped $SrTiO_3$.

3.3. Band structure and density of states

The band structure for undoped and doped systems for the 40-atom supercell is shown in Fig.3 for $BaTiO_3$ and in Fig.4 for $SrTiO_3$ respectively. The band gap values are listed in Table 3. From Fig.3(a), we could observe that the top of valence band and the bottom of conduct band lie at R point and Γ point of Brillouin zone respectively. So the pure $BaTiO_3$ crystal is an indirect gap insulator. The theoretical indirect gap at Γ–R is 1.80 eV, which is slightly smaller than the direct band gap of 1.87 eV at Γ point, see Table 3. However, the band gaps are significantly reduced in the Fe-doped $BaTiO_3$ system because of the appearance of the defect band. The band gap changes to the Γ–X point of Brillouin zone, which is still an indirect gap. Consequently, the gap is reduced to 1.23 eV, which is 0.56 eV smaller than the undoped bulk indirect gap. Correspondingly, the direct gap at Γ point in a dopant system also reduces to 1.54 eV, which is 0.33 eV smaller than the corresponding bulk value. As for the Fe-doped $SrTiO_3$ system, the general features are qualitatively the same as those for the Fe-doped $BaTiO_3$. Due to the defect energy band, the position of the indirect band gap shifts to a new position (Γ–X), and the gap value reduces from 1.85 eV to 1.43 eV in the Fe-doped $SrTiO_3$ 40-atom system. The reductions of indirect and direct gaps are 0.42 and 0.41 eV, respectively. The reduction of the indirect band gap for $SrTiO_3$ (0.42 eV) is slightly smaller than that for $BaTiO_3$ (0.56 eV). This implies that the Fe impurity has a stronger influence on the band gap of $BaTiO_3$ than on that of $SrTiO_3$.

Table 3. The band gap value of $BaTiO_3$ and $SrTiO_3$.

	$BaTiO_3$		$StTiO_3$	
bulk	Γ–R	1.80	Γ–R	1.85
	Γ–Γ	1.87	Γ–Γ	2.18
40-atom	Γ–X	1.23	Γ–X	1.43
	Γ–Γ	1.54	Γ–Γ	1.77

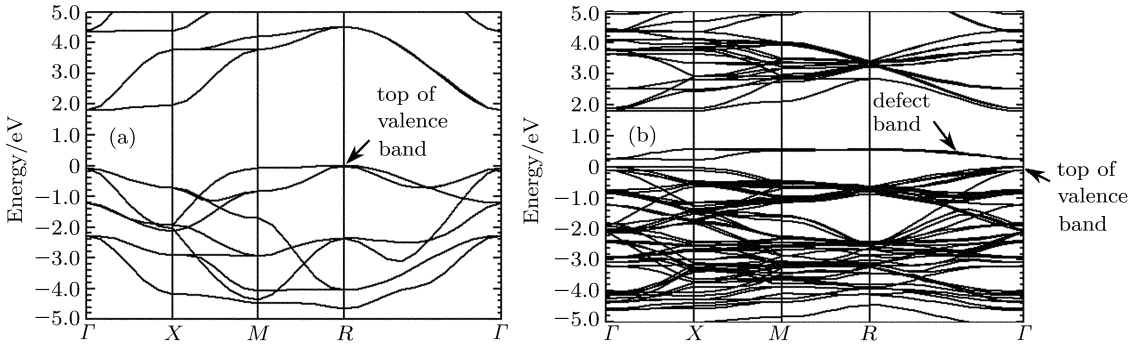


Fig.3. The band structure: (a) undoped $BaTiO_3$, (b) a single Fe impurity in a 40-atom $BaTiO_3$ supercell. The top of valence is set to be zero.

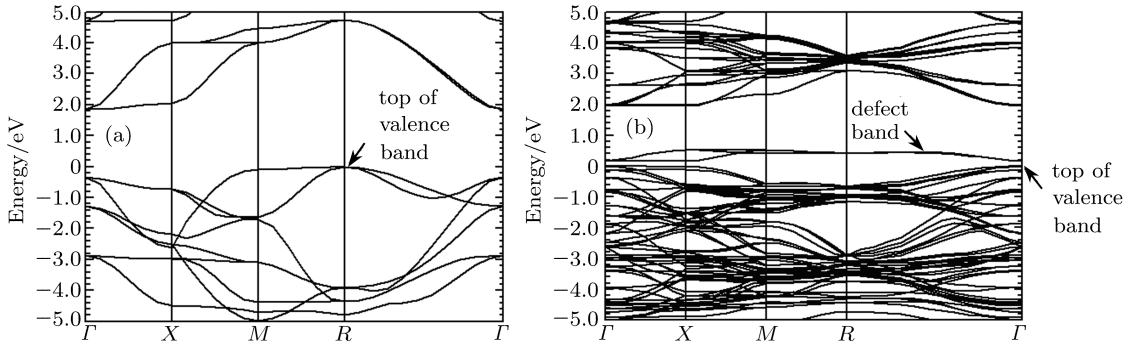


Fig.4. The band structure: (a) undoped $SrTiO_3$, (b) a single Fe impurity in a 40-atom $SrTiO_3$ supercell. The top of valence is set to be zero.

In undoped $BaTiO_3$ and $SrTiO_3$ structures, the lowest conduction band is quite flat from Γ to X, which is a common feature of many ABO_3 perovskite ferroelectrics. From Fig.3(b) and Fig.4(b), we can see that the defect band appears between the conduct and valences band, but is closer to the valence band. Although there is a remarkable change of the lower conduction bands as shown in Fig.3(b) and Fig.4(b), the lowest conduction band between the Γ and X points is not significantly affected by the Fe doping. For $BaTiO_3$, the defect band dispersion is weak throughout the Brillouin zone, and the bandwidth is about 0.3 eV. The most distinct dispersion lies at the X point. In the case of $SrTiO_3$, the most distinct dispersion also lies at the X point with a bandwidth about 0.35 eV, which is slightly larger than that of $BaTiO_3$.

The total density of states (DOSs), the partial DOSs of the Fe impurity, and the partial DOSs of its nearest ions (O, Ba, Ti) in 40-atom $BaTiO_3$ supercell are displayed in Fig.5. We present only the DOSs of $BaTiO_3$ system because of the similarity between Fe-doped $BaTiO_3$ and $SrTiO_3$ systems. These DOSs demonstrate that the valence band mainly consists of the Fe 3d, O 2p, Ti 3d and Ba 5p electrons. The main contribution to the conduction band comes from Fe 3d and Ti 3d electrons. The most important feature in Fig.5 is that there appears a sharp peak near the Fermi energy in the total DOS, corresponding to the defect band in Fig.3(b). From the partial DOSs, we can easily see that this sharp peak in the total DOS mainly comes from the effect of Fe impurity. The amplitude of the main Fe 3d peak is about 16 states/eV. Owing to the hybridization with Fe, the DOS of O 2p near the Fermi energy rises to 1.4 states/eV. The DOS of Ti 3d also has a slight change as well: going up to 0.1 states/eV around the Fermi energy. All these lead to the appearance of the new peak near the Fermi energy in the total DOS.

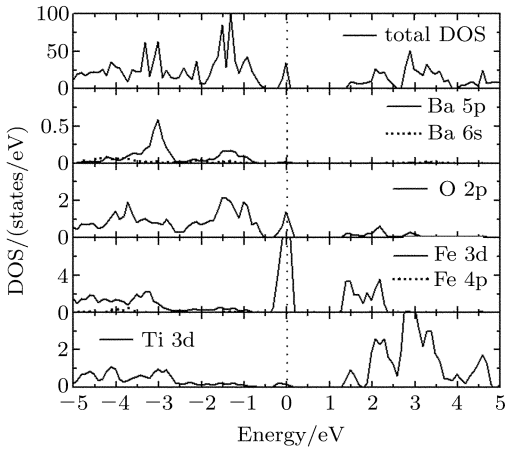


Fig.5. The total DOS, partial DOS of Fe impurity and its nearest atoms. The Fermi energy is set to be zero.

4. Conclusion

With the LDA-PWP scheme, the structural and electronic properties of the Fe-doped $BaTiO_3$ and $SrTiO_3$ have been studied. Firstly, we have found that the dopant formation energy is 6.8 eV for Fe-doped $BaTiO_3$ and 6.5 eV for Fe-doped $SrTiO_3$ systems respectively. Secondly, the distances between Fe impurity and its nearest O atoms and between Fe impurity and Ba or Sr atoms become small by comparison with those of the corresponding undoped bulk systems. The shrinkage of the Fe–O distance is about 1%. Thirdly, we have obtained the Fe defect energy band, which mainly originates from Fe 3d electrons by analysing the DOS.

References

[1] Gunter P and Huignard J P (ed) 1998 *Photorefactive Materials and their Application I and II* (Berlin: Springer)

[2] Waser R, Bieger T and Maier J 1990 *Solid State Commun.* **76** 1077

[3] Wang W T, Yang G, Duan P, Zhou Y L and Chen Z H 2002 *Chin. Phys. Lett.* **19** 1122

[4] Ang C, Yu Z, Jing Z, Lunkenheimer P and Loidl A 2000 *Phys. Rev.* B **61** 3922

[5] Higuchi T, Tsukamoto T, Kobayashi K, Ishiwata I, Fujisawa M, Yokoya T, Yamaguchi S and Shin S 2000 *Phys. Rev.* B **61** 12860

[6] Liu Q B, Li R Q, Zeng Y Z and Zhu Z Z 2006 *Acta Phys. Sin.* **55** 0873 (in Chinese)

[7] Yao M Z, Gu M and Liu F S 2003 *Chin. Phys.* **12** 0084

[8] Liu F S, Gu M and Zhang R 2004 *Chin. Phys.* **13** 1931

[9] Selme M O, Pecheur P and Toussaint G 1984 *J. Phys.* C **17** 5185

[10] Michel-Calendini F M and Muller K A 1981 *Solid State Commun.* **40** 255

[11] Evarestov R A, Piskunov S, Kotomin E A and Borstel G 2003 *Phys. Rev.* B **67** 064101

[12] Astala R and Bristowe P D 2001 *Modelling Simul. Mater. Sci. Eng.* **9** 415

[13] Benthem van K, Elsasser C and French R H 2001 *J. Appl. Phys.* **90** 6156

[14] Shi W S, Chen Z H, Liu N N, Liu H B, Zhou Y L, Cui D F and Chen Z H 1999 *Appl. Phys. Lett.* **75** 1547

[15] Yang G, Wang H H, Tan G T, Jiang A Q, Zhou Y L, Yang G Z and Chen Z H 2001 *Chin. Phys. Lett.* **18** 1598

[16] Zhang W F, Huang Y B, Zhang M S and Liu Z G 2000 *Appl. Phys. Lett.* **76** 1003

[17] Baroni S, Corso D A, Gironcoli S, Giannozzi P, Cavazzoni C, Ballabio G, Scandolo S, Chiarotti G, Focher P, Pasquarello A, Laasonen K, Trave A, Car R, Marzari N and Kokalj A http://www.pwscf.org/

[18] Perdew J P and Zunger A 1981 *Phys. Rev.* B **23** 5048

[19] Vanderbilt D 1990 *Phys. Rev.* B **41** 7892

[20] Monkhost H J and Pack J D 1976 *Phys. Rev.* B **13** 5188

[21] Hellwege K H and Hellwege A M 1969 *Ferroelectrics and Related Substances,* New Series Group III Vol.**3** (Berlin: Spinger)

[22] Kim L, Kim J, Waghmare U V, Jung D and Lee J 2005 *Phys. Rev.* B **72** 214121

[23] Kim L, Kim J, Jung D, Lee J and Waghmare U V 2005 *Appl. Phys. Lett.* **87** 052903

[24] Cantele G, Degoli E, Luppi E, Magri T, Ninno D, Iadonisi G and Ossicini S 2005 *Phys. Rev.* B **72** 113303